RESEARCH ARTICLE

ADVANCED OPTICAL MATERIALS
www.advopticalmat.de

Near-Infrared Lifetime Nanothermometry Detects Microwave-Induced Brain Heating

*Liyan Ming, José Lifante, Ginés Lifante Pedrola, Daniel Ortega, Irene Zabala-Gutierrez, Jorge Rubio-Retama, Erving Ximendes, Riccardo Marin, Julio Ramiro Bargueño, and Daniel Jaque**

In modern environments, the brain is continuously exposed to numerous external stimuli, including the microwave radiation used in telecommunication technologies. It has been suggested that the absorption of this radiation by brain tissue can induce local heating. Because brain temperature influences neural activity, metabolism, and overall brain function, microwave-induced heating raises concerns over the safety of such technologies. Proper evaluation of the risks associated with microwave-based technologies thus requires accurate quantification of heating in deep organs without disrupting their physiology. This study, demonstrates that microwave-induced brain heating can be remotely monitored in vivo via luminescence thermometry using near-infrared luminescent silver sulfide (Ag_2S) nanoparticles. Their temperature-dependent luminescence lifetime is a reliable thermometric parameter for the measurement of absolute brain temperature. The in vivo results offer direct, real-time evidence of brain heating (up to 4 °C) under telecom exposure conditions (3 GHz). Moreover, they establish lifetime thermometry as a reliable, minimally invasive approach for investigating thermoregulation in deep tissues even under external electromagnetic stimulation.

1. Introduction

Brain temperature is a critical physiological parameter that directly influences neural function, neuron metabolic activity, and overall brain homeostasis. Even slight deviations in temperature can significantly affect cognitive performance, synaptic transmission, and neuronal excitability,[1,2] with repercussions on our quality of life. In the modern era, the blooming of technologies based on electromagnetic radiation in the telecommunication band (0.3-300 GHz, **Figure 1**) introduces external stimuli that may alter brain temperature and, consequently, impact the health of individuals.[3,4] Microwave (MW) frequencies used in wireless communication, particularly in the 2–3 GHz range, are known to be efficiently absorbed by water (Figure 1), which, coincidentally, is the main constituent of brain tissues (>70%).[5–8] Thus, brain is an organ especially susceptible to

L. Ming, J. Lifante, G. L. Pedrola, E. Ximendes, R. Marin, D. Jaque
Nanomaterials for Bioimaging Group (nanoBIG)
Departamento de Física de Materiales
Facultad de Ciencias
Universidad Autónoma de Madrid
Madrid 28049, Spain
E-mail: daniel.jaque@uam.es

L. Ming, J. Lifante, E. Ximendes
Nanomaterials for Bioimaging Group (nanoBIG)
Instituto Ramón y Cajal de Investigación Sanitaria (IRYCIS)
Hospital Ramón y Cajal
Madrid 28034, Spain

L. Ming, R. Marin, D. Jaque
Instituto de Ciencia de Materiales Nicolás Cabrera
Universidad Autónoma de Madrid
Madrid 28049, Spain

The ORCID identification number(s) for the author(s) of this article can be found under https://doi.org/10.1002/adom.202502319

DOI: 10.1002/adom.202502319

D. Ortega
Condensed Matter Physics department, Faculty of Sciences
Campus Universitario de Puerto Real
Puerto Real, Cádiz 11510, Spain

D. Ortega
INiBICA - Instituto de Investigación e Innovación Biomédica de Cádiz
Biomedical Research and Innovation Institute of Cádiz
Cádiz 11009, Spain

D. Ortega
IMDEA Nanoscience
Faraday 9, Madrid 28049, Spain

I. Zabala-Gutierrez, J. Rubio-Retama
Department of Chemistry in Pharmaceutical Sciences, Pharmacy Faculty
Complutense University of Madrid
Madrid 28040, Spain

R. Marin, D. Jaque
Institute for Advanced Research in Chemical Sciences (IAdChem)
Universidad Autónoma de Madrid
Madrid 28049, Spain

J. Ramiro Bargueño
Department of Signal Theory and Communications, Telematics and Computing
Universidad Rey Juan Carlos
Madrid 28943, Spain

MW-induced heating, which could result in disruption of neuronal signaling, induction of oxidative stress, and a reduction in the integrity of the blood-brain barrier.[9–11]

Proper evaluation of how telecom radiation-induced heating affects neural function and long-term health requires access to brain temperature. Yet, current methods for intracranial temperature measurement present inherent limitations. Invasive techniques that rely on macroscopic sensors, like thermocouple implantation, disrupt normal physiology and introduce readout artifacts.[12] Non-invasive methods such as functional magnetic resonance-based approaches lack the spatial and temporal resolution necessary for dynamic temperature readout.[13] Thus, the development of real-time, remote thermal sensing methods is imperative for both fundamental neuroscience research and safety assessments of emerging technologies.

One candidate technology for intracranial thermal sensing at the in vivo level is near-infrared (NIR) luminescence thermometry, which makes use of so-called NIR luminescence nanothermometers (NIR-LNThs)–i.e., luminescent species with temperature-dependent luminescence. Among NIR-LNThs, silver sulfide (Ag_2S) nanoparticles stand out in terms of thermometric performance and biocompatibility.[14–19] Ag_2S NIR-LNThs have been used for in vivo luminescence thermometry, including lifetime-based approaches. This methodology offers improved reliability compared to spectral luminescence thermometry methods,[17] which are inherently plagued by tissue-induced spectral distortions.[14] Despite these promising features, the application of lifetime-based Ag_2S NIR-LNThs to brain temperature monitoring remains unexplored.

In this work we optimize a lifetime-based nanothermometry approach to achieve precise temperature monitoring of brain in living animals exposed to telecommunication band MW radiation.

2. Results and Discussion

The Ag_2S nanoparticles used in this work were synthesized by a previously-reported thermal decomposition method,[20] and subsequently dispersed in water by surface modification with poly (ethylene glycol) as described in the Experimental Section.[21] Transmission electron microscopy (TEM) observations reveal monodispersed spherical nanoparticles with an average diameter of 4.1 ± 0.6 nm (Figure S1, Supporting Information). Dynamic light scattering (DLS) measurements yield a hydrodynamic size of ≈13.5 nm in phosphate buffered saline (PBS).[22] For the calibration of Ag_2S nanoparticles as lifetime-based NIR-LNThs, a colloidal dispersion (1 mg mL^{-1} in PBS) was placed into a temperature-controlled holder that allows optical excitation with a picosecond 634 nm laser and detection of emitted intensity with a photon-counting photomultiplier (**Figure 2a**). The absorption and photoluminescence (PL) spectra (see Figure S2, Supporting Information) confirm the expected optical properties of the Ag_2S nanoparticles, validating the suitability of 634 nm as the excitation wavelength. The resulting emission lies in the NIR-II window, supporting their applicability for deep-tissue temperature sensing. Thermal quenching of the emission generated by Ag_2S NIR-LNThs is evidenced by an acceleration in the luminescence decay rate (Figure 2b). Indeed, the average luminescence lifetime ($\bar{\tau} = \int_0^\infty I(t)tdt \,/\, \int_0^\infty I(t)dt$, where $I(t)$ is the emission intensity at time t after laser excitation) decreases monotonously with temperature (Figure 2c), in agreement with previous reports on Ag_2S NIR-LNThs.[23,24] The relative sensitivity ($S_r\,(T) = \bar{\tau}(T)^{-1}\,|\frac{\partial\bar{\tau}}{\partial T}|$) of Ag_2S NIR-LNThs as lifetime-based NIR-LNThs is close to 4% $°C^{-1}$ in the physiological temperature range (Figure 2d).[25] This thermal sensitivity – among the highest reported for lifetime based thermal sensors (see comparative Table S1, Supporting Information) – anticipate thermal readouts with low associated thermal uncertainty, ($\delta T = S_r(T)^{-1} \cdot \delta\bar{\tau}$, where $\delta\bar{\tau}$ is the uncertaintity in the determination of the average lifetime).

To verify the robustness of Ag_2S NIR-LNThs as lifetime-based NIR-LNThs their fluorescence decay curves were recorded during consecutive heating-cooling cycles from 20 to 48 °C. The luminescence lifetime remains consistent across cycles (Figure 2e), with repeatability (see Section S1, Supporting information) of ≈92%. The lifetime of Ag_2S LNThs is also robust against pH variations (Figure 2f), nanoparticle concentration (Figure 2g), and long-term 634-nm picosecond laser irradiation (Figure 2h). To that end, the results reported in Figure 2h also demonstrate how this type of laser irradiation does not damage the Ag_2S LNThs nor does it induce thermal loading. The absence of laser-induced thermal loading in this situation is, indeed, reasonable since the pulse duration is shorter than the characteristic electron-phonon coupling time (<ps).[26] The use of picosecond irradiation represents thus an advantage over the nanosecond pulse excitation used in previously reported in vivo lifetime sensing experiments.[27,28]

Finally, the possibility that Ag_2S NIR-LNThs could undergo MW-induced heating was also explored. Dried Ag_2S NIR-LNThs deposited on a glass slide were continuously exposed to MW radiation (3 GHz, 1.2 W cm^{-2}) while detecting luminescence lifetime and monitoring temperature via thermal camera. The luminescence lifetime of Ag_2S NIR-LNThs under MW excitation remains constant within a 1% confidence interval (51.1 ± 0.6 ns, see Figure 2i). According to the calibration curve of Figure 2c, lifetime data indicates that the temperature of our Ag_2S NIR-LNThs remains constant at 20.6 ± 0.3 °C, in accordance with the thermal readouts provided by the thermal camera (Figure 2i).

Prior to in vivo experiments, the reliability of Ag_2S as lifetime-based NIR-LNThs for monitoring MW-induced heating within tissues was tested by performing experiments using brain phantoms. In these experiments, the conditions of subsequent in vivo experiments are mimicked. Details about the fabrication of brain phantoms are given in the Supporting Information. For these experiments, 6 µL of a PBS dispersion of Ag_2S NIR-LNThs (5 mg mL^{-1}) was injected into the brain phantom at a depth of 4 mm and the fluorescence lifetime was continuously

J. Lifante
Neuroimmunology Lab, Department of Neurology and Neurosurgery, The Montreal Neurological Institute (MNI)
McGill University
3801 University Road, Montreal, QC H3A 2B4, Canada
R. Marin
Intelligent Optical Nanomaterials (IONs), Dipartimento di Scienze Molecolari e Nanosistemi (DSMN)
Università Ca' Foscari Venezia
Venezia-Mestre 30170, Italy

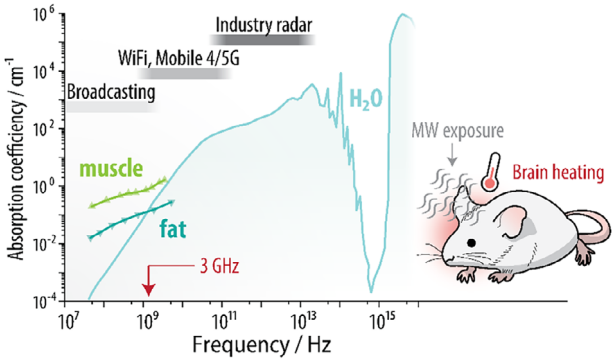

Figure 1. Frequency-dependent electromagnetic absorption in biological systems. The operating spectral ranges in which different technologies operate are indicated.

measured during irradiation with a MW antenna. The surface temperature of the brain phantom is simultaneously recorded with an infrared thermal camera (**Figure 3a**). The images obtained with the thermal camera reveal how the surface temperature of the brain phantom increases with the frequency of MW radiation (Figure 3b, corresponding to a MW power density of 1.2 W cm^{-2}), in agreement with the absorption spectra of tissues reported in the 1–3 GHz spectral range (Figure 1).[7] For a 3 GHz frequency—a mid-band frequency used in 5G telecommunications—we achieve the maximum heating in our experimental conditions. The magnitude of surface heating increases monotonously with irradiation time and reaches a *plateau* value after 5 min of irradiation (Figure 3c, data obtained for 3 GHz frequency). Irradiation for longer times does not lead to further heating; therefore 5 min was selected as the irradiation time for the subsequent in vivo experiments. The magnitude of surface heating increases monotonously with the power density of the MW radiation (Figure 3d), as expected due to the increment of the total energy absorbed by water molecules within the brain phantom. The internal temperature of the phantom during continuous MW irradiation is monitored by acquiring the luminescence decay curves of the injected Ag_2S NIR-LNThs (Figure 3e). As soon as the MW antenna is switched ON, the fluorescence lifetime of Ag_2S NIR-LNThs starts decreasing (Figure 3f), denoting an instantaneous internal heating of the brain phantom. The conversion of lifetime data into temperature (based on the calibration curve included in Figure 2c) reveals that the internal temperature also reaches a plateau after 5 min of MW irradiation, with the magnitude of heating increasing with the MW power density (Figure 3g,h). Although surface and internal temperature show similar trends, they present differences when they are compared for the same MW power intensity (Figure 3g). The internal temperature is consistently higher than the one measured at the phantom's external surface by the infrared thermal camera. This reduced temperature increment at the surface of the brain phantoms was expected, since heat dissipation to the environment leads to an overall lower average surface temperature. The time evolution of both internal and surface temperature as well as the difference between internal and surface temperature are in accordance with numerical simulations (solid lines in Figure 3g and Section S5, Supporting Information). This agreement supports the use of lifetime-based Ag_2S NIR-LNThs for reliable in situ monitoring of the internal temperature of brain in the presence of MW telecommunication radiation.

After having validated the suitability of the proposed thermometric approach during MW irradiation in brain phantoms and confirming the low cytotoxicity of PEG-functionalized Ag_2S nanothermometers through in vitro assays (see Figure S3, Supporting Information), we aimed to test the possibility of measuring brain heating caused by 3 GHz MW radiation in an in vivo model. A bolus of Ag_2S NIR-LNThs in PBS (10 mg mL^{-1}, 6 µL) was injected into the brain of a living mouse at a depth of 4 mm (**Figure 4a**). Details about the injection procedure are given in Experimental Section. The anesthetized mouse was placed close to the microwave antenna, which produced a MW power density of 611 W m^{-2} at the location where the mouse's head laid (Figure S5, Supporting Information). The optical system for NIR-LNThs excitation and signal collection as well as the procedure for the analysis of the luminescence decay curves were the same as those described above in Figure 2 and Figure 3. Decay curves of Ag_2S NIR-LNThs were acquired before and after 5 min of MW irradiation revealing a decrease in the average lifetime from 31.1 ± 0.4 down to 26.9 ± 0.3 ns (Figure 4b). According to the calibration curve (Figure 2c), these lifetime values correspond to an increase of intracranial temperature from 34.8 ± 0.2 up to 39.4 ± 0.2 °C after 300 s of 3 GHz MW irradiation (Figure 4c). These experimental values agree with those obtained via in silico models – Section S5 of the Supporting Information (Figures S6 and S7, Supporting Information) describes in detail the conditions adopted in our numerical calculations. Specifically, in silico thermal images before and after microwave irradiation (600 W m^{-2}, 3 GHz, 300 s) also reveal a brain temperature increment at a given intracranial depth of 4 mm, from 34.5 up to 39.3 °C (Figure 4d; Figures S8 and S9, Supporting Information). Hence, both experimental measurements and simulations indicate an intracranial temperature increase close to 4 °C. Thermal camera measurements under similar conditions showed lower temperature rises (≈0.8 °C, Figure S10, Supporting Information), revealing that the MW-induced heating is larger at intracranial locations than at the surface (skin): this observation is in agreement with in silico experiments (Figure S9, Supporting Information). The total 3 GHz MW power reaching the brain was estimated (assuming a cross-sectional area of $3.7 \cdot 10^{-4}$ m^2) to be 0.22 W. This leads to an intracranial heating rate of 17 °C W^{-1} that is of the same order of magnitude, but significantly larger, than the MW-induced heating rates in tissues reported in the literature (see Table S2, Supporting Information). The larger heating rate obtained here can be explained by the fact that it was evaluated for 3 GHz whereas previous works in the literature evaluated the heating rate at 2.45 GHz where absorption is sizably lower (Figure 1 and Figure 3b). The heating rate determined from both in vivo and in silico experiments can be used to estimate the heating effect caused, for instance, by the 3 GHz radiation generated by a smart phone. Considering that a smart phone can generate 0.2 W (similar to the total MW power reaching the mouse head in our in vivo experiments) and taking into account that the mass of human brain is 10^3 times that of a mouse, our results anticipate an intracranial temperature increment in a human brain well below 0.1 °C. This is, indeed, in agreement with previous reports who suggested that under normal usage conditions, smart phones are expected to cause intracranial heating below 0.3 °C.[29]

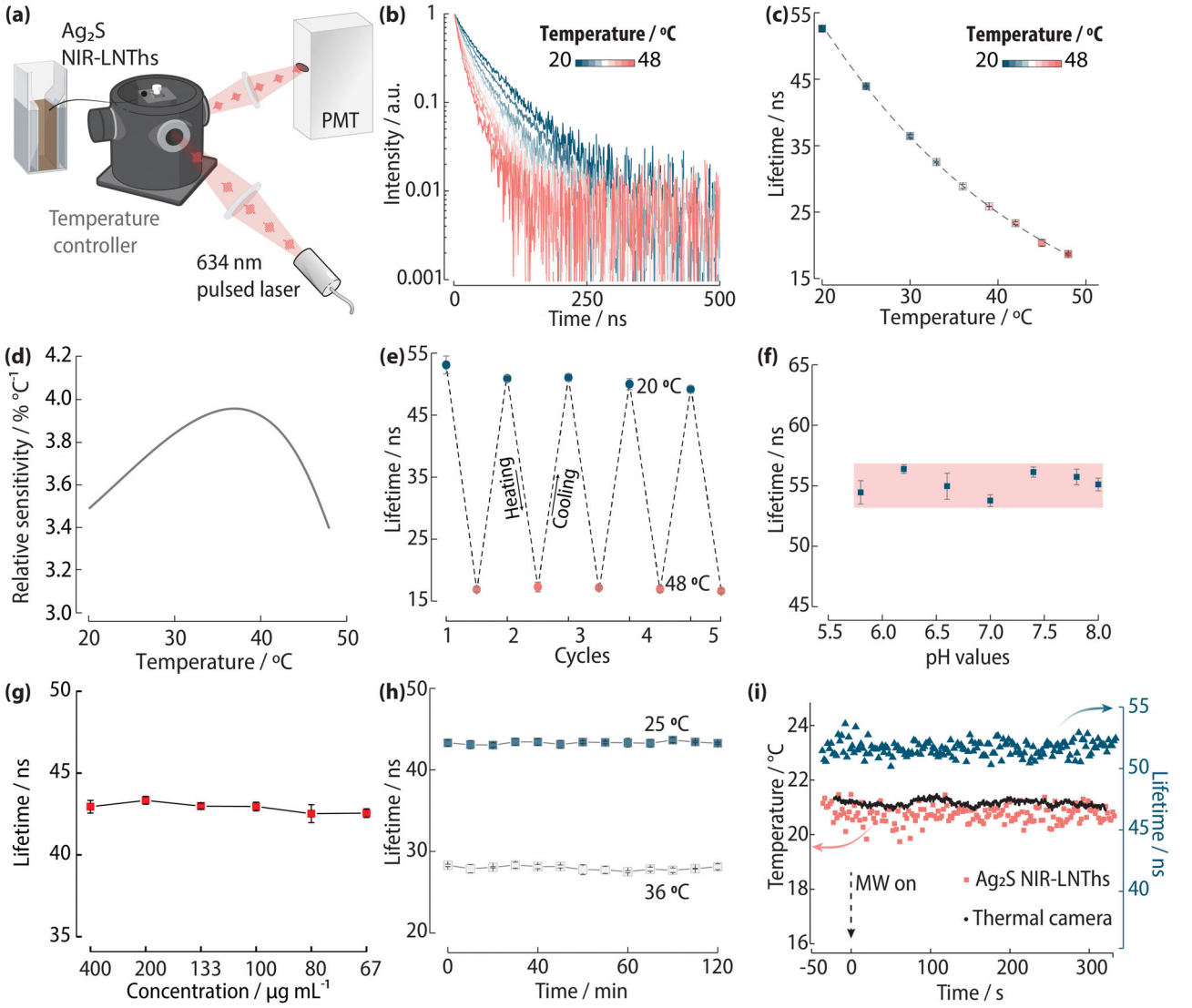

Figure 2. Characterization of Ag_2S lifetime-based LNThs for reliable temperature measurements under MW irradiation. a) Scheme of the experimental setup system used to calibrate the NIR-LNThs as a function of temperature (T). b) Luminescence decay curves collected at different temperatures from an Ag_2S NIR-LNThs dispersion in PBS (1 mg mL^{-1}). c) Temperature dependence of the average lifetime ($n = 3$) of Ag_2S NIR-LNThs extracted from the decays curves reported in b) The fitting curve follows the expression $\tau = 98.8252 - 2.7256T + 0.02197T^2$, with $R^2 = 0.9997$. d) Temperature dependence of lifetime-based relative thermal sensitivity of Ag_2S NIR-LNThs. e) Luminescence lifetime of Ag_2S NIR-LNThs ($n = 3$) at 20 and 48 °C obtained after consecutive heating and cooling cycles. f) Lifetime of Ag_2S NIR-LNThs ($n = 3$) obtained in aqueous dispersions at different pH values (pH 5.8–8, at 20 °C). g) Lifetime of Ag_2S NIR-LNThs ($n = 3$) obtained in aqueous dispersions with different nanoparticle concentrations (400–67 mg mL^{-1}, at 25 °C). h) Luminescence lifetime of Ag_2S NIR-LNThs ($n = 3$) at 25 and 36 °C obtained under continuous picosecond laser irradiation. i) Comparison of the lifetime-derived temperatures of a powder sample of Ag_2S NIR-LNThs under MW exposure. The thermal readout provided by the thermal camera is also included.

The observed intracranial temperature rise of ≈4 °C may have physiological implications. Literature reports suggest that even moderate brain hyperthermia—on the order of 1–3 °C—can influence neural excitability, synaptic activity, and cerebral blood flow, especially in thermosensitive brain regions.[1,30] Acute heating above 3 °C has been associated with increased metabolic demand, oxidative stress, and alterations in neurotransmitter signaling—although such changes are generally reversible if exposure is brief. Conversely, sustained or repeated thermal stress may compromise blood–brain barrier function and initiate neuroinflammatory pathways.[31,32] These findings underscore the importance of monitoring and controlling temperature in studies involving electromagnetic exposure.

3. Conclusion

In conclusion, in this work we have demonstrated the viability of lifetime-based infrared nanothermometry—specifically using Ag_2S NIR-LNThs—for monitoring in vivo brain temperature during exposure to telecommunication radiation. Experiments

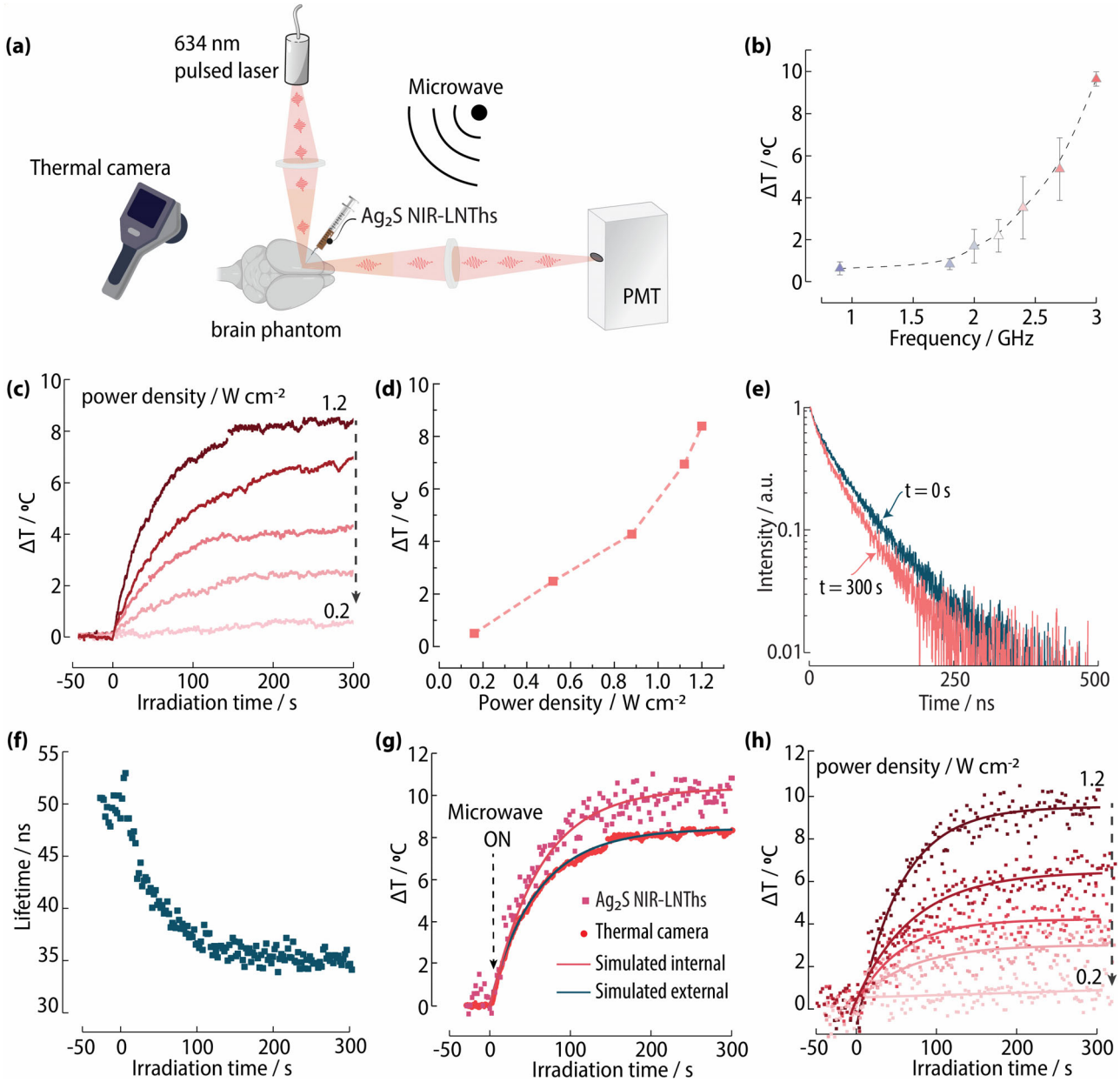

Figure 3. Validation of lifetime-based Ag_2S NIR-LNThs for thermal monitoring of brain in the presence of telecom radiation. a) Scheme of the experimental setup for monitoring the microwave-induced heating of a brain phantom. Surface temperature is recorded by a thermal camera whereas internal temperature is obtained from the analysis of the fluorescence lifetime of Ag_2S NIR-LNThs that were injected into the brain phantom. b) Surface heating in a brain phantom caused by microwave irradiation of different frequencies and monitored by thermal camera ($n = 3$). The power density of microwave radiation and irradiation time were set to 1.2 W cm^{-2} and 5 min, respectively. c) Time evolution of phantom brain surface temperature and d) increased temperature after 5 min caused by 3 GHz microwave radiation as obtained for different power densities. e) Luminescence decay curves before ($t = 0$ s) and after microwave radiation ($t = 300$ s). f) Time evolution of the average lifetime of Ag_2S NIR-LNThs during microwave (3 GHz, 1.2 W cm^{-2}) radiation. g) Internal and surface heating of a brain phantom caused by microwave (3 GHz, 1.2 W cm^{-2}) radiation. Internal temperature calculated from f) base on the calibration curve in Figure 2c, while surface temperature is provided by an infrared thermal camera. Simulated surface and internal temperature of brain phantom. h) Time evolution of the increment in the internal temperature of brain phantom monitored by Ag_2S NIR-LNThs during microwave (3 GHz) radiation with different power densities. The solid lines are the exponential fitting curves of the scatters.

conducted in brain phantoms revealed a clear dependence of microwave-induced heating on irradiation parameters such as time, frequency, and power. In vivo studies corroborated these findings, quantifying a heating rate of ≈17 °C W^{-1} for 3 GHz radiation. Although in vivo experiments were conducted under conditions leading to larger exposure to MW radiation than those typically encountered in daily life, the proportionality between deposited energy and temperature rise allows extrapolation of our results. Considering the lower power density of common devices and the larger brain mass in humans, our data suggest that brain

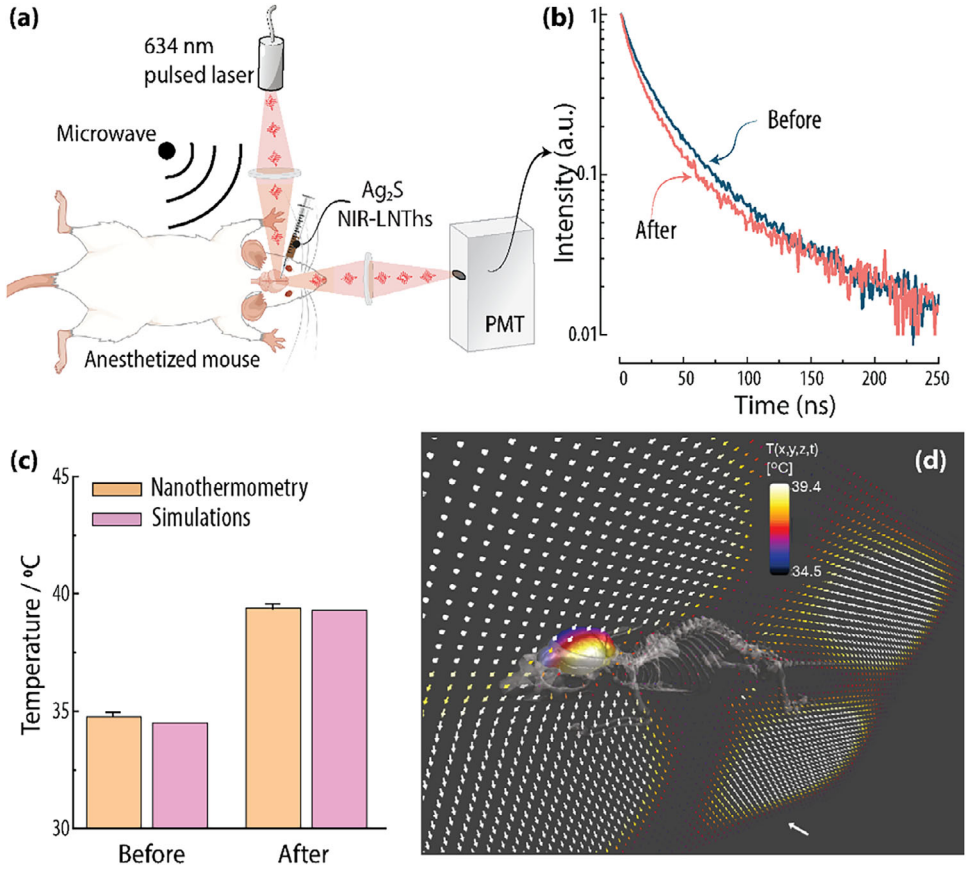

Figure 4. In vivo experimental determination of intracranial heating caused by microwave telecommunication radiation: comparison with the in silico model. a) Scheme of the experimental set-up used for measuring microwave-induced brain heating in small animals using Ag_2S lifetime-based nanothermometers. b) Infrared luminescence decay curves of Ag_2S NIR-LNThs located within the brain as measured before and after microwave irradiation (3 GHz, 611 W m^{-2}, 300 s of irradiation). c) Brain temperature before and after MW irradiation as obtained from the analysis of the luminescence decay curves included in b). d) Virtual mouse model overlaid with a volumetric temperature map showing the transient heating produced by the 3 GHz, 604 W m^{-2} microwave irradiation after 300 s, and the corresponding **E** vector field. White-to-red arrows distributed throughout the sagittal plane depict the local direction of the **E** field, while the larger solid white arrow at bottom indicates the incident field's propagation direction toward the animal from the antenna. The average brain temperatures at a depth of 4 mm obtained in each case are also included in c) for the sake of comparison with the experimental data.

heating under normal telecommunication exposure is expected to remain below 0.1 °C.

This work not only confirms the occurrence of brain heating due to telecommunication radiation but also introduces a novel, minimally invasive technique for brain thermometry. Lifetime-based infrared nanothermometers hold significant promise for the development of diagnostic tools and for the precise control of brain thermal therapies in both research and clinical settings.

4. Experimental Section

Chemical Reagents: Silver nitrate (99,9%), sodium diethyldithiocarbamate (NaDDTC) (ACS reagent grade) and 1-dodecanethiol (≤98%) (DDT) were purchased from Sigma–Aldrich. -metoxi–mercapto PEG (CH_3O-PEG-SH, MW = 2000 Da) are from RAPP Polymere. Organic solvents such as chloroform (CHCl3) (99.6%), ethanol absolute pure (99.8%) and diethyl ether (99.5%) were acquired at PanReac AppliChem.

Synthesis of Ag_2S-PEG NIR-LNThs: The synthesis of NIR-LNThs was performed as previously described and comprised two sequential steps: i) preparation of Ag_2S NIR-LNThs in organic media and ii) subsequent transfer of the nanoparticles to water.[1]

Ag_2S NIR-LNThs were obtained via thermal decomposition of the single-source precursor silver diethyldithiocarbamate (AgDDTC). AgDDTC was first synthesized by reacting $AgNO_3$ (4.25 g, 25 mmol) with NaDDTC (5.63 g, 25 mmol), each dissolved in 200 mL of Milli-Q water. Addition of the NaDDTC solution to the $AgNO_3$ solution yielded a yellow precipitate that was collected by vacuum filtration and dried at 60 °C for later use.

For nanoparticle formation, AgDDTC (25 mg, 0.10 mmol) and 1-dodecanethiol (DDT; 5 mL, 20.5 mmol) were placed in a round-bottom flask at room temperature. The mixture was sonicated under vacuum for 10 min to remove residual air and moisture, then purging with nitrogen. It was heated to 185 °C at 20 °C min^{-1} under gentle magnetic stirring, held at this temperature for 1 h, and allowed to cool naturally. The resulting NIR-LNThs were purified by adding ethanol (10 mL) to destabilize the dispersion and centrifuging at 10 000 g for 10 min; this washing step was repeated twice. The purified Ag_2S NIR-LNThs were finally redispersed in $CHCl_3$ at 1 mg mL^{-1}.

Transfer to aqueous media was achieved by ligand exchange between surface-bound DDT and poly (ethylene glycol) (PEG). HS-PEG-MeO (5 mg, Mw = 2000 Da) was added to 1 mL of the $CHCl_3$ dispersion to

obtain charge-neutral NIR-LNThs in water. The mixture was sonicated for 5 min at room temperature to promote PEG grafting. PEGylated nanoparticles were precipitated with diethyl ether and collected by centrifugation at 2000 g for 2 min. The pellet was redispersed in 500 µL of ethanol and 500 µL of Milli-Q water; ethanol was then removed by evaporation, and the PEGylated Ag_2S NIR-LNThs were finally suspended in 1 mL of Milli-Q water.

Tissue (brain) Phantom Fabrication: An aliquot of 9.9 mL Tris-HCl buffer (pH 6.8) and 0.1 mL Intralipids were mixed in a single neck flask (50 mL) and placed in an oil bath set on a magnetic heating stirrer. The mixture was heated to 110 °C under stirring, then 100 mg agar was added into this emulsion. Subsequently, the dispersion was kept at 110 °C under continuous stirring for 15 min to ensure complete dissolution of the agar. While still hot, it was poured into a brain-shaped mold and left to cool to room temperature, whereupon it gelled completely. Once the gel had solidified, the phantom was carefully removed from the mold. In this formulation, Intralipid functions as the optical scatterer that replicates the light-diffusing properties of biological tissue, whereas agar forms the structural matrix that imparts the desired mechanical integrity to the phantom.

Acquisition of Fluorescence Decay Curves: Luminescence decay curves were measured using time-correlated single photon counting (TCSPC) on a Timeharp 260 time-correlated single photon counting module (PicoQuant) and with a photo multiplier tube (PMT) detector (H10330C, HAMAMATSU) to capture the fluorescence photons. The samples were excited using a pulsed laser (EPL-640, Edinburgh Instruments) at a wavelength of 634 nm, with a pulse width of 100 ps and a repetition rate of 2 MHz. To obtain the decay curve, the samples were excited with the pulsed laser and the photoluminescence was detected by the PMT detector and a 1050 nm long pass filter placed in front of the PMT. The resulting photon arrival times were recorded using the Timeharp module. For measurements of the temperature calibrations, we used a Peltier-based temperature-controlled cuvette holder (Qpod 2e, Quantum Northwest, Inc.) to vary the tempearture of an Ag_2S NIR-LNTh dispersion in water (1 mg mL^{-1})from 20 to 48 °C. The fluorescence decay curves at different temperatures were measured by Timeharp 260 board (PicoQuant) with a integration time of 5 s.

Microwave Generator: Signal generation was performed with a generator Hitite HMC-T2000 SYNTHESIZED SIGNAL GENERATOR with range of measurement 900 MHz to 3 GHz. The output of the signal generator is connected to the input of a broadband amplifier model R&SBBA150 broadband amplifiers that covers frequencies between 0.69 to 3.2 GHz and with a maximum output power of 30 W.

The signal was radiated by means of an EM-6961 Double Ridged Guide Antenna which was a linearly polarized broadband antenna designed and built specifically for EMI measurements and specification compliance testing capable of operating either a transmitting or receiving antenna. It was well suited for radiated susceptibility testing in the microwave range. It was constructed of rugged aluminum, which makes it excellent for use under severe field conditions and the size makes it suitable for use in the limited space of a shielded enclosure.

The verification of the generated signal both in frequency and power was performed using a Rohde & Schwarz FSH20 Handheld Spectrum Analyzer, and with a Narda FieldMan – electromagnetic field meter using a Probe EFD-0692, E-Field; 600 MHz-6 GHz.

Cytotoxicity Assay: To assess the biocompatibility of the PEG-functionalized Ag_2S nanoparticles, a standard MTT assay was performed using U87 MG cells. Cells were seeded into 96-well plates and incubated with increasing concentrations of Ag_2S nanoparticles (ranging from 0 to 250 µg mL^{-1}) for 24 h. After incubation, MTT reagent (0.5 mg mL^{-1}) was added and cells were incubated for an additional 1.5 h. The resulting formazan crystals were dissolved in Dimethyl sulfoxide (DMSO), and absorbance was measured at 570 nm using a microplate reader. Cell viability was calculated relative to untreated control cells.

In Vivo Experiments: For this study, female C57/BL6 mice (n = 1) were purchased from Charles River Laboratories (6 weeks-old) and were housed in specific pathogen-free (SPF) conditions ad libitum for 2 weeks prior to experiments for acclimation period. This strain was selected due to the hairless phenotype, allowing increased imaging resolution due to reduction in autofluorescence background coming from pigmented melanins naturally present in the fur. The in vivo experiments carried out in this work were approved by the Ethics Committee from Universidad Autónoma de Madrid (CEI) and Comunidad de Madrid (PROEX 58.7-23) and complied with:

1) The local Ethics Committee for Animal Research at the host institution according to regional and national regulations. The investigation conforms to the Guide for the Care and Use of Laboratory Animals published by the European Parliament (EU directive 2010/63/EU).

2) The royal ordinance RD 53/2013, February 1, which establishes the basic rules applicable for the protection of animals during experimental and other scientific purposes, including teaching.

3) The order ECC/566/2015, March 20, establishes the training requisites that the personnel handling, breeding, or providing animals for experimentation or teaching has to fulfil according to the Spanish legislation.

4) The Transparency Committees of the Universidad Autónoma de Madrid (UAM), Universidad Complutense de Madrid, and the Autonomic Government of Madrid (PROEX 58.7-23) based on the statement supporting European Directive 2010/63/EU on the protection of animals used for scientific purposes. These Committees are created by the European institution EARA.

To deliver Ag_2S NIR-LNThs into the brain parenchyma, a stereotaxic injection system (Nanopump Elite 11, Harvard Apparatus) was used to slowly inject 6 µL of Ag_2S NIR-LNThs (10 mg mL^{-1}) with a 33 Gauge stereotaxic flexible syringe under a controlled flow with a total duration of 5 min. During the injection and subsequent experimental procedure, the animals were anesthetized and carefully monitored using inhaled isoflurane (Micro digital anesthesia system, Kent Scientific, anesthesia induction.

During the detection period, the animals were anaesthetized under isoflurane anesthesia (4.5% isoflurane for induction and 1.5%–2% isoflurane to maintain anesthetic plane; O_2 levels were adjusted by the anesthetic system based on mice weight (23–25 g average / mouse). Sufficient anesthetic depth was assessed at the beginning of the procedure and continuously monitored each 10 min by certifying the absence of mouse paw reflexes after a nociceptive pitch stimulus. Also, mice temperature was monitored and maintained at (37.5 ± 1.0) °C throughout the entire experiment using a thermal blanket coupled to the homeothermic monitoring system of the microdigital anesthesia. Finally, animals were euthanized at the end of the experiment through beheading after an isoflurane overdose (5% isoflurane during 5 min prior to euthanasia).

To demonstrate the suitability of Ag_2S NIR-LNThs to monitor intracranial temperature, we selected a considerable injection depth: for this reason, the intracerebral location chosen were subcortical structures (Anteroposterior AP -1.0 mm, Medial-lateral ML -1.0 mm, Dorsoventral DV -4.0 mm). During the injection and subsequent experimental procedure, the animals were anesthetized using inhaled isoflurane (Micro digital anesthesia system, Kent Scientific) and positioned in a stereotaxic frame with the head aligned and securely fixed. The injection site was first marked by positioning the needle at the target coordinates. The needle was then retracted, and a small cranial opening was made using a drill at the marked point (Microdrill, 10,000 rpm, Harvard apparatus). Bone fragments were carefully removed and dural rupture was visually confirmed using a stereotaxic dissection system. The needle was reinserted at the same site and lowered to the target depth using the depth control shaft. To ensure proper retention of the NIR-LNThs at the site, the needle was first advanced an additional 0.2 mm beyond the target depth to create a tissue "pocket" and then retracted back to 4 mm before prior the injection. The injection system administered the solution steadily until the full 6 µL volume was delivered. Following the injection, the needle was left in place for an additional 2 min to allow the NIR-LNThs to stabilize within the tissue. Finally, the needle was withdrawn very slowly to minimize backflow.

Statistical Analysis: Temperature and lifetime uncertainties were calculated as the standard deviation (SD) of repeated measurements. The sample size (n) for each measurement was indicated in the corresponding figure legends. No additional statistical tests were applied. All data processing and analysis were performed using [Origin 2019].

Supporting Information

Supporting Information is available from the Wiley Online Library or from the author.

Acknowledgements

This work has been supported by Spanish Ministry of Science. The authors acknowledge support under grants PID2020- 117544RB-I00, PID2021-123318OB-I00 and CEX2020-001039-S funded by MCIN/AEI/10.13039/501100011033 and by the Comunidad Autónoma de Madrid (TEC-2024COM-360 DISCO-6G-CM) grant and co-financed by the European structural and investment fund. The authors would like to express the gratitude to the Electromagnetic Compatibility Area of the "Instituto Nacional de Técnica Aeroespacial" (INTA) for the loan of the antenna for these experiments. The authors were grateful for the support of ZMT Zurich MedTech AG, the developer of the software used for the simulations reported in this work, Sim4Life, www.sim4life.swiss. L.M. acknowledges a scholarship from the China Scholarship Council (No. 202108350018). E.X. thanks the Community of Madrid for funding the project SI4/PJI/2024-00130 through a direct grant with Universidad Autónoma de Madrid, and also acknowledges support from grant RYC2023-044309-I, funded by MICIU/AEI (10.13039/501100011033) and the FSE. R.M. is grateful to the Spanish Ministerio de Ciencia, Innovación y Universidades for support to research through a Ramón y Cajal Fellowship (RYC2021-032913-I) and Project 102R0103 (NAMSTEPS) funded by MICIU/AEI/10.13039/501100011033 and by FEDER, EU.

Conflict of Interest

The authors declare no conflict of interest.

Data Availability Statement

The data that support the findings of this study are available from the corresponding author upon reasonable request.

Keywords

heating, luminescence lifetime, luminescence thermometry, microwave radiation, thermal effects

Received: July 18, 2025
Revised: October 13, 2025
Published online: November 6, 2025

[1] E. A. Kiyatkin, P. L. Brown, R. A. Wise, *Eur. J. Neurosci.* **2002**, *16*, 164.
[2] M. Volgushev, T. R. Vidyasagar, M. Chistiakova, U. T. Eysel, *Neuroscience* **2000**, *98*, 9.
[3] S. Banik, S. Bandyopadhyay, S. Ganguly, *Bioresour. Technol.* **2003**, *87*, 155.
[4] D. Raković, Eds. O. Gouni, J. R. G. Turner, T. G. N. Turner, in: Change: Birthing and Parenting at Times of Crisis, Cosmoanelixis & Int. J. of Prenatal & Life Sciences, Athens, Invited Chapter 3, **2021**.
[5] D. Misra, *Radio-Frequency and Microwave Communication Circuits: Analysis and Design*, John Wiley & Sons, **2001**.
[6] N. H. Ishak, R. Ariffin, A. Ali, M. A. Sagiruddin, F. Mohamad Twon Tawi, in *2011 IEEE International Conference on Control System, Computing and Engineering*, IEEE, Penang, Malaysia, **2011**, pp. 551–556.
[7] G. Ku, B. D. Fornage, X. Jin, M. Xu, K. K. Hunt, L. V. Wang, *Technol. Cancer Res. Treat* **2005**, *4*, 559.
[8] K. R. Foster, A. Lozano-Nieto, P. J. Riu, T. S. Ely, *Bioelectromagnetics* **1998**, *19*, 420.
[9] S. Mumtaz, J. N. Rana, E. H. Choi, I. Han, *Int. J. Mol. Sci.* **2022**, *23*, 9288.
[10] W.-J. Zhi, L.-F. Wang, X.-J. Hu, *Military Med Res* **2017**, *4*, 29.
[11] D. R. Justesen, *Proc. IEEE* **1980**, *68*, 60.
[12] U. Izhar, L. Piyathilaka, D. M. G. Preethichandra, *Neurosci. Inform.* **2022**, *2*, 100106.
[13] J. Klohs, W. C. Chen, R. Araki, *npj Imaging* **2025**, *3*, 27.
[14] Y. Shen, J. Lifante, N. Fernández, D. Jaque, E. Ximendes, *ACS Nano* **2020**, *14*, 4122.
[15] Y. Shen, H. D. A. Santos, E. C. Ximendes, J. Lifante, A. Sanz-Portilla, L. Monge, N. Fernández, I. Chaves-Coira, C. Jacinto, C. D. S. Brites, L. D. Carlos, A. Benayas, M. C. Iglesias-de la Cruz, D. Jaque, *Adv. Funct. Mater.* **2020**, *30*, 2002730.
[16] H. D. A. Santos, E. C. Ximendes, M. D. C. Iglesias-de La Cruz, I. Chaves-Coira, B. Del Rosal, C. Jacinto, L. Monge, I. Rubia-Rodríguez, D. Ortega, S. Mateos, J. GarcíaSolé, D. Jaque, N. Fernández, *Adv Funct Mater.* **2018**, *28*, 1803924.
[17] Y. Shen, J. Lifante, I. Zabala-Gutierrez, M. Fuente-Fernández, M. Granado, N. Fernández, J. Rubio-Retama, D. Jaque, R. Marin, E. Ximendes, A. Benayas, *Adv. Mater.* **2022**, *34*, 2107764.
[18] E. C. Ximendes, U. Rocha, B. Del Rosal, A. Vaquero, F. Sanz-Rodríguez, L. Monge, F. Ren, F. Vetrone, D. Ma, J. García-Solé, C. Jacinto, D. Jaque, N. Fernández, *Adv Healthc. Mater.* **2017**, *6*, 1601195.
[19] B. Del Rosal, D. Ruiz, I. Chaves-Coira, B. H. Juárez, L. Monge, G. Hong, N. Fernández, D. Jaque, *Adv. Funct. Mater.* **2018**, *28*, 1806088.
[20] A. Ortega-Rodríguez, Y. Shen, I. Z. Gutierrez, H. D. A. Santos, V. T. Vera, E. Ximendes, G. Villaverde, J. Lifante, C. Gerke, N. Fernández, O. G. Calderón, S. Melle, J. Marques-Hueso, D. Mendez-Gonzalez, M. Laurenti, C. M. S. Jones, J. M. López-Romero, R. Contreras-Cáceres, D. Jaque, J. Rubio-Retama, *ACS Appl. Mater. Interfaces* **2020**, *12*, 12500.
[21] S. Mateos, J. Lifante, C. Li, E. C. Ximendes, T. Muñoz-Ortiz, J. Yao, M. De La Fuente-Fernández, Á. L. G. Villalón, M. Granado, I. Zabala Gutierrez, J. Rubio-Retama, D. Jaque, D. H. Ortgies, N. Fernández, *Small* **2020**, *16*, 1907171.
[22] S. Yang, Y. Liu, Y. Wang, A. Cao, *Small* **2013**, *9*, 1635.
[23] L. Ming, I. Zabala-Gutierrez, P. Rodríguez-Sevilla, J. R. Retama, D. Jaque, R. Marin, E. Ximendes, *Adv. Mater.* **2023**, *35*, 2306606.
[24] H. D. A. Santos, D. Ruiz, G. Lifante, C. Jacinto, B. H. Juarez, D. Jaque, *Nanoscale* **2017**, *9*, 2505.
[25] S. F. Collins, G. W. Baxter, S. A. Wade, T. Sun, K. T. V. Grattan, Z. Y. Zhang, A. W. Palmer, *J. Appl. Phys.* **1998**, *84*, 4649.
[26] R. R. Gattass, E. Mazur, *Nat. Photon* **2008**, *2*, 219.
[27] J. K. Chen, W. P. Latham, J. E. Beraun, *J. Laser Appl.* **2005**, *17*, 63.
[28] R. L. Harzic, N. Huot, E. Audouard, C. Jonin, P. Laporte, S. Valette, A. Fraczkiewicz, R. Fortunier, *Appl. Phys. Lett.* **2002**, *80*, 3886.
[29] D. Bhargava, N. Leeprechanon, P. Rattanadecho, T. Wessapan, *Int. J. Heat Mass Transfer* **2019**, *130*, 1178.
[30] M. Rango, A. Arighi, N. Bresolin, *NeuroReport* **2012**, *23*, 483.
[31] S. Mrozek, F. Vardon, T. Geeraerts, *Anesthesiol. Res. Pract.* **2012**, *2012*, 989487.
[32] E. A. Kiyatkin, H. S. Sharma, *Neuroscience* **2009**, *161*, 926.